JACS
JOURNAL OF THE AMERICAN CHEMICAL SOCIETY
pubs.acs.org/JACS
Article

Methanetriol—Formation of an Impossible Molecule

Joshua H. Marks, Xilin Bai, Anatoliy A. Nikolayev, Qi'ang Gong, Cheng Zhu, N. Fabian Kleimeier, Andrew M. Turner, Santosh K. Singh, Jia Wang, Jiuzhong Yang, Yang Pan, Tao Yang,* Alexander M. Mebel,* and Ralf I. Kaiser*

Cite This: J. Am. Chem. Soc. 2024, 146, 12174−12184
Read Online
ACCESS | Metrics & More | Article Recommendations | Supporting Information

ABSTRACT: Orthocarboxylic acids—organic molecules carrying three hydroxyl groups at the same carbon atom—have been distinguished as vital reactive intermediates by the atmospheric science and physical (organic) chemistry communities as transients in the atmospheric aerosol cycle. Predicted short lifetimes and their tendency to dehydrate to a carboxylic acid, free orthocarboxylic acids, signify one of the most elusive classes of organic reactive intermediates, with even the simplest representative methanetriol ($CH(OH)_3$)—historically known as orthoformic acid—not previously been detected experimentally. Here, we report the first synthesis of the previously elusive methanetriol molecule in low-temperature mixed methanol (CH_3OH) and molecular oxygen (O_2) ices subjected to energetic irradiation. Supported by electronic structure calculations, methanetriol was identified in the gas phase upon sublimation via isomer-selective photoionization reflectron time-of-flight mass spectrometry combined with isotopic substitution studies and the detection of photoionization fragments. The first synthesis and detection of methanetriol ($CH(OH)_3$) reveals its gas-phase stability as supported by a significant barrier hindering unimolecular decomposition. These findings progress our fundamental understanding of the chemistry and chemical bonding of methanetriol, hydroxyperoxymethane (CH_3OOOH), and hydroxyperoxymethanol ($CH_2(OH)OOH$), which are all prototype molecules in the oxidation chemistry of the atmosphere.

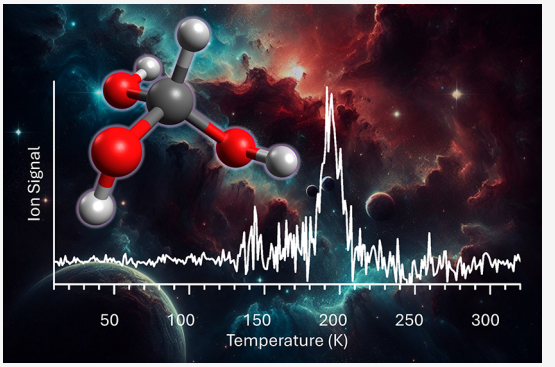

1. INTRODUCTION

Since the formulation of the Erlenmeyer rule stating that organic compounds carrying more than one hydroxyl (−OH) group on the same carbon atom are not stable and tend to split off water by Emil Erlenmeyer almost 150 years ago, the preparation of geminal diols ($R_2C(OH)_2$), orthocarboxylic acids ($RC(OH)_3$), and orthocarbonic acid (methanetetrol; $C(OH)_4$) containing multiple hydroxyl groups on the same carbon atom has challenged the synthetic, theoretical, and physical organic chemistry communities. This is driven by interest in fundamental chemical bonding and electronic structure theory, along with their potential as atmospheric and astrochemical reaction intermediates.[1−10] These ortho acids ($RC(OH)_3$) are thermodynamically unstable due to the greater binding energy of a carbon−oxygen double bond relative to two carbon−oxygen single bonds, in addition to the steric repulsion of the adjacent hydroxyl groups. Steric repulsion represents a common motif in methanediol ($CH_2(OH)_2$), methanetriol ($CH(OH)_3$), and methanetetrol ($C(OH)_4$) (Figure 1), of which only methanediol has been detected in the gas phase.[11]

Although methanetriol (**1**, $CH(OH)_3$) has remained undetected, its structural isomers hydroxyperoxymethane (**2**, CH_3OOOH) and hydroxyperoxymethanol (**3**, $CH_2(OH)OOH$) represent critical combustion intermediates and are ubiquitous in the troposphere (Scheme 1).[1−3,5−8,10] Tropospheric and stratospheric **2** results from reactions between methane (CH_4) and abundant hydroxyl ($\dot{O}H$).[3,5,8−10,12,13] Though short-lived with estimated lifetimes of 20 ps in the troposphere, this species is a major source of reactive molecules like singlet oxygen ($^1O_2$), formaldehyde (H_2CO), and hydrogen peroxide (H_2O_2).[3,5,8−10,12−18] Reactions of atmospheric ozone (O_3) with alkenes produce Criegee intermediates (RR′COO), which are a major driving force behind atmospheric chemistry, aerosol growth, and a critical source of ambient hydroxyl ($\dot{O}H$) radicals contributing in turn to the formation of **2**.[19] Hydration of methylidene(oxido)-oxidanium (H_2COO), the simplest Criegee intermediate, then produces **3**.[4,6,7,20−24]

It has been predicted computationally that the elusive **1** requires energetic initiation, such as photochemically activated processes, to form. All three CH_4O_3 isomers are thermody-

Received: February 22, 2024
Revised: April 1, 2024
Accepted: April 2, 2024
Published: April 17, 2024

https://doi.org/10.1021/jacs.4c02637
J. Am. Chem. Soc. 2024, 146, 12174−12184

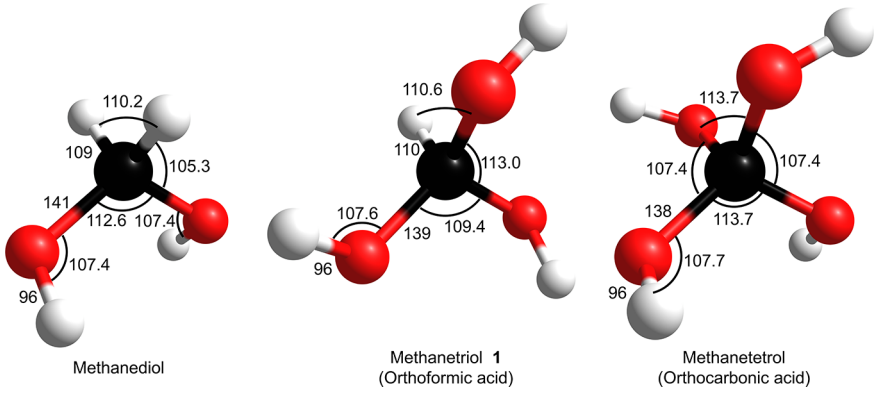

Figure 1. Structures of the lowest energy conformers of methanediol[11] (C_2, $CH_2(OH)_2$), methanetriol (C_1, $CH(OH)_3$), and methanetetrol (S_4, *trans–gauche–gauche*, $C(OH)_4$) showing bond lengths (pm) and angles (degrees). Structural parameters are omitted where redundant.

Scheme 1. This Investigation Explores the Synthesis of CH_4O_3 Isomers, and Particularly of Methanetriol (1) in Extreme Environments in Low Temperature Ices. Combustion Reactions are a Well-Documented Source of Hydroxyperoxymethane (2), and the Atmospheric Reactions of Criegee Intermediates Have Been Shown to Produce Hydroxyperoxymethanol (3), an Important Source of Environmental Formaldehyde

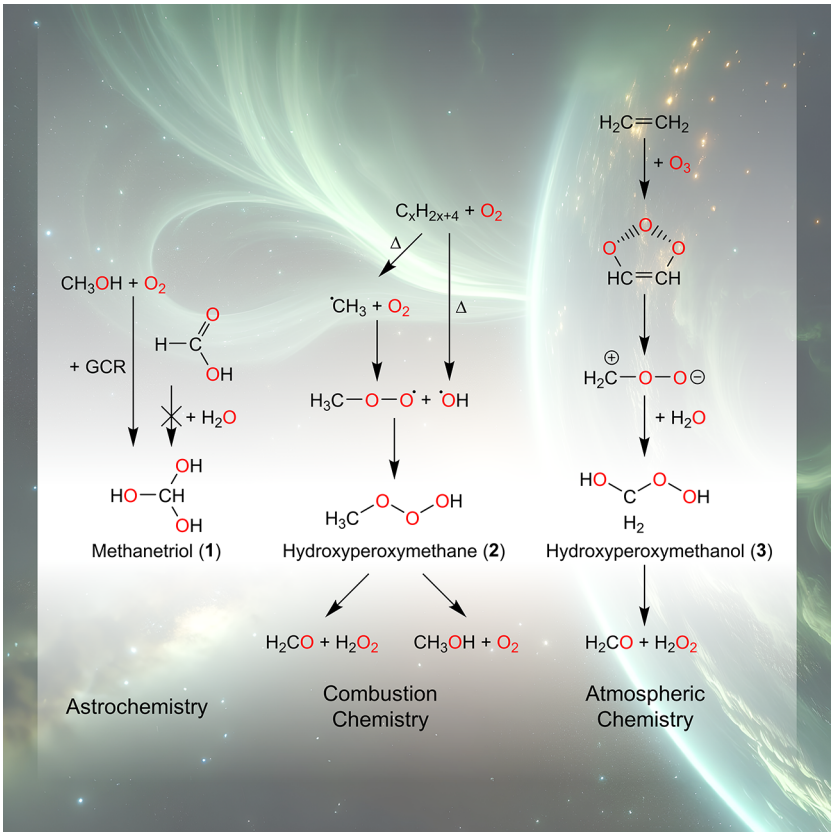

namically unstable with regard to unimolecular decomposition to products like methanol (CH_3OH) plus molecular oxygen (O_2) or H_2CO and H_2O_2.[3,13,25−36] In the presence of an acidic or basic catalyst, **1** can dehydrate via proton transfer, making its formation or isolation a significant challenge for traditional synthetic protocols.[32] A recent computational investigation revealed that the dehydration of **1** to formic aid (HCOOH) is exoergic by 39 kJ mol^{-1}; however, a significant barrier of 148 kJ mol^{-1} highlights the kinetic stability of **1** toward gas-phase unimolecular decomposition. Therefore, computational studies predict that **1** should be detectable once prepared in a sufficiently cold environment.[35] Considering these energetics and the limits imposed by environmental conditions, free orthocarboxylic acids ($RC(OH)_3$), particularly prototype compound **1**, represent one of the most elusive groups of transient organic molecules. This system is also of fundamental interest from the viewpoint of chemical bonding and electronic structure theory to benchmark the chemical reactivity and critical bond-breaking processes leading to orthocarboxylic acids in extreme environments, such as on ice-coated nanoparticles in cold molecular clouds and in the low-temperature stratosphere.

Here, we present the preparation of methanetriol (**1**) along with its isomers hydroxyperoxymethane (**2**) and hydroxyper-

https://doi.org/10.1021/jacs.4c02637
J. Am. Chem. Soc. 2024, 146, 12174−12184

Scheme 2. Schematic Representation of Reactions in Ices of Methanol and Molecular Oxygen (CH_3OH-O_2) Leading Toward Isomers of CH_4O_3. Adiabatic Ionization Energies of 1−3 Shown are Representative of the Range of Ionization Energies Predicted for all Conformers Identified

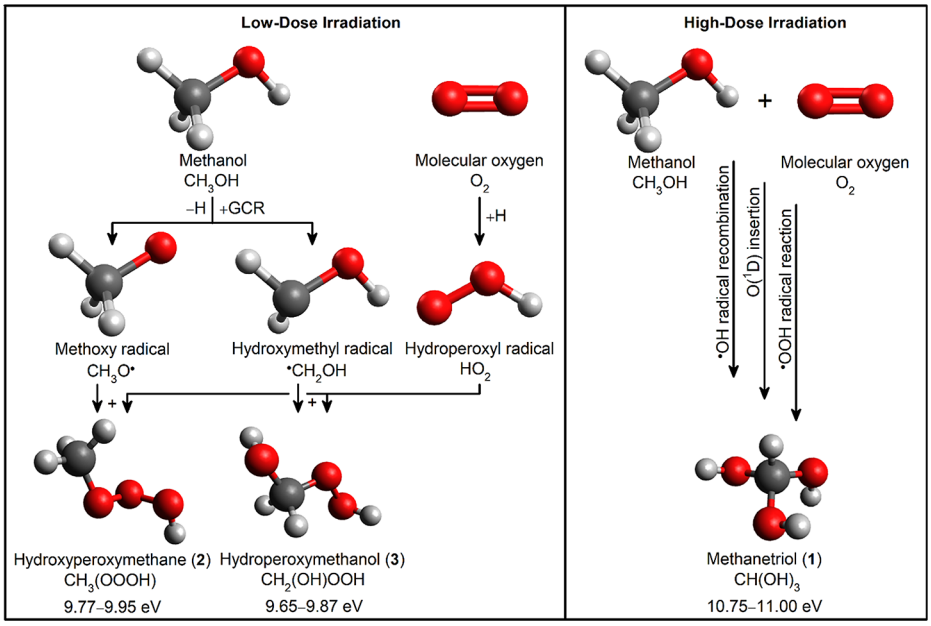

oxymethanol (**3**) in low-temperature (5 K) methanol−molecular oxygen (CH_3OH-O_2) ices exposed to energetic electrons as proxies of energetic galactic cosmic rays (GCRs).[37] All three isomers were uniquely identified in the gas phase upon sublimation during temperature-programmed desorption (TPD), exploiting vacuum ultraviolet (VUV) photoionization coupled with reflectron time-of-flight mass spectrometry (Re-ToF-MS). While isotopic labeling aids in the identification of the molecular formula, computational predictions of isomer-specific dissociative photoionization pathways allow the use of these fragmentation processes for discrimination between isomers **1**−**3**. The detection of **1**, the simplest orthocarbonic acid ($RC(OH)_3$), has significant consequences for research in atmospheric chemistry since the orthocarboxylic acid group is expected to participate in the formation of atmospheric organic aerosol particles;[35] however, organics as small as these are not major drivers of aerosol growth, which requires large low-volatility organics to promote condensation.[38] The oxygen-dense functional groups of **1**−**3** allow them to serve as prototype molecules in the examination of atmospheric oxidative chemistry. Molcecule **1** is the simplest possible orthocarbonic acid, a class of molecules that may represent a reservoir of atmospheric carboxylic acids. In particular, stratospheric ice particles exhibit an environment that may be conducive to the formation and preservation of orthocarboxylic acids. Their facile decomposition may constitute a major source of the unaccounted-for atmospheric abundance of formic and acetic (CH_3COOH) acids.[39,40] Considering the vital role these acids play in cloud formation, the presence of atmospheric **1** further has the potential to affect global climate and rain patterns.[39] Overall, the existence of **1** and its isomers (**2** & **3**) documented here connects the chemistry of hydroperoxides (ROOH), hydroxyperoxides (ROOOH), orthocarbonic acids, and carboxylic acids (RCOOH) with Criegee intermediates; their study delivers new knowledge on the complex chemistry of our planet's atmosphere and potentially any oxygen-rich exoplanet, with the novel synthesis of **1** opening the possibility of studying the undoubtedly unique chemistry of this exotic species and its derivatives.[1,3,5,6,8,10,23]

2. RESULTS

2.1. Computations. The presence of electron-withdrawing groups such as hydroxyl (−OH) in a molecule has a strong tendency to promote dissociation in radical cations driven by the thermodynamically favorable separation of a radical and cation.[41,42] It is therefore vital to anticipate potential dissociative channels of the radical cations through computational quantum chemical assessment of methanetriol ($\mathbf{1}^{\bullet+}$), hydroxyperoxymethane ($\mathbf{2}^{\bullet+}$), and hydroperoxyl-methanol ($\mathbf{3}^{\bullet+}$). Gas-phase calculations carried out at the CCSD(T)/CBS//ωB97X-D/aug-cc-pVTZ level of theory identify three neutral structural isomers **1**−**3** (Scheme 2). Conformers of the investigated species are labeled with letters indicating only their relative energies, where **1a** is the minimum energy conformer of **1**, and this *trans*−*gauche*−*gauche* (*tgg*, C_1) conformer is separated from the *gauche*−*gauche*−*gauche* conformer **1b** (*ggg*, C_s, +5 kJ mol^{-1}) by a low barrier of 9 kJ mol^{-1} (Figure S1 and Table S1). A *trans*−*gauche*−*gauche*′ conformer, **1c** (*tgg*′, C_3, 10 kJ mol^{-1}), is only metastable. Adiabatic ionization of **1**—ionization into the ground electronic, vibrational, and conformational radical cation state—is expected to result in prompt dissociation by loss of atomic hydrogen. While a transition state is identified as a saddle-point on the potential energy surface, after the addition of zero-point vibrational energy (ZPVE) corrections, the energy of this transition state becomes lower than that of $\mathbf{1a}^{\bullet+}$, the minimum-energy radical cation conformer (Figure S2 and Table S2); consequently, there is no effective barrier to dissociation yielding a hydrogen atom (Ḣ) and the trihydroxymethylium cation ($C(OH)_3^+$). If this ionization process occurs, it should produce a signal at the mass-to-charge ratio m/z = 63. Vertical ionization—ionization into the radical cation conformer most structurally similar to the neutral—may

https://doi.org/10.1021/jacs.4c02637
J. Am. Chem. Soc. 2024, 146, 12174−12184

not result in prompt dissociation. Figure 2 shows that conformer $\mathbf{1b}^{\bullet+}$ faces a 6 ± 4 kJ mol^{-1} barrier to dissociation,

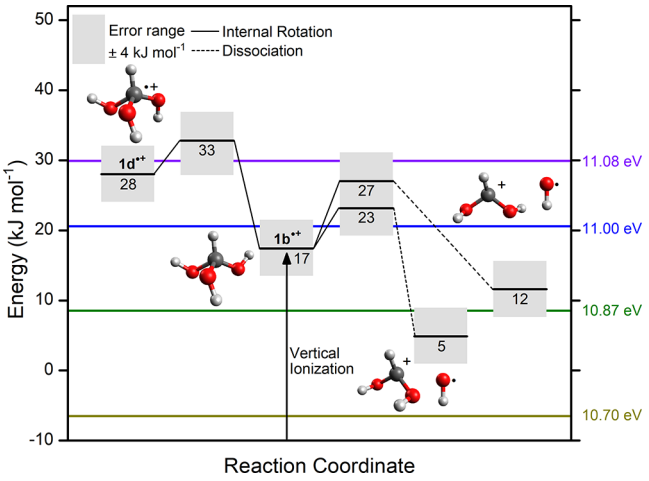

Figure 2. Potential energy surface for $CH(OH)_3^+$. Vertical ionization of **1** is separated by a small barrier from dissociation to yield $CH(OH)_2^+$. Gray rectangles represent an error of ±4 kJ mol^{-1}. Dashed lines show dissociative unimolecular reaction pathways. Energy (kJ mol^{-1}) is relative to the minimum energy radical cation conformational isomer of **1**.

yielding the dihydroxymethylium cation ($CH(OH)_2^+$). The errors intrinsic to these calculations and the barrier height are so similar that it is indeterminate whether this molecule possesses a bound radical cation state or must dissociate when formed. If dissociation occurs from this conformer, **1** can be detected by the presence of fragment ions at m/z = 47 and potentially at m/z = 64 for the parent. Accounting for the Stark effect and thermal energy of the subliming neutrals from the ice, the calculated ionization energies presented here include a −0.03 eV correction. With this correction, the threshold for adiabatic ionization into the $\mathbf{1a}^{\bullet+}$ state and the appearance energy of $C(OH)_3^+$ are 10.79 ± 0.04 eV, vertical ionization into the $\mathbf{1b}^{\bullet+}$ state at 10.97 ± 0.04 eV, and the appearance energy of the $CH(OH)_2^+$ fragment is 11.03 ± 0.04 eV. Since this computational analysis shows that **1** will likely undergo dissociative photoionization, this information is crucial for both the planning and analysis of experiments that can identify the presence of **1**.

The computational investigation of the radical cation dissociation dynamics of hydroxyperoxymethane (**2**) and hydroperoxymethanol (**3**) reveals that both isomers are substantially more robust toward dissociative photoionization. Molecule **2** is found to have only two conformers differing in energy by 10 ± 4 kJ mol^{-1}, which have a possible adiabatic ionization energy within the range of 9.77−9.95 eV (Figure S3). The energy necessary to cleave the $[H_3CO{-}OOH]^{\bullet+}$ bond between hydroperoxyl (ȮOH) and protonated formaldehyde (H_2COH^+) is predicted to be 198 kJ mol^{-1} for the most stable cation ($\mathbf{2a}^{\bullet+}$), which is the result of adiabatic or vertical ionization of **2a**. There is no identified transition state between the reactant and products for this unimolecular reaction, and the energy increases monotonically as the OO bond is elongated. An appearance energy of 11.96 ± 0.04 eV is anticipated for H_2COH^+ if it is produced by **2**. Conversely, the dissociation channel to produce these same fragments from $\mathbf{3}^{\bullet+}$ requires the cleavage of the CO bond rather than an OO bond. For this isomer, adiabatic ionization of any of the six conformers is expected with photons of 9.65−9.87 eV (Table S1). The dissociation process requires only 84 kJ mol^{-1} in excess of adiabatic ionization with an appearance energy of 10.70 ± 0.04 eV, which is in agreement with the experimental value of 10.6−10.7 eV.[7] The overlapping ranges for the possible adiabatic ionization energies of **2** (9.77−9.95 eV) and **3** (9.65−9.87 eV) prevent using photon energy alone for isomer-selective photoionization; however, the fragmentation of the nascent ions can be used as a powerful tool to unambiguously distinguish between methanetriol and its isomers.

2.2. Mass Spectrometry. Mass spectra produced using photoionization reflectron time-of-flight mass spectrometry (PI-ReToF-MS) and temperature-programmed desorption (TPD) of irradiated methanol-molecular oxygen ($CH_3OH{-}O_2$) ices are shown in Figure 3. In the blank (unirradiated) experiment, only the methanol cation (CH_3OH^+) was detected. Since organic species featuring substitution by electron-withdrawing substituents such as hydroxyl groups on the same carbon atom are unstable as radical cations and face a small barrier to dissociation yielding a radical and a closed-shell cation,[41,42] the aforementioned electronic structure calculations provide the only vital way to assess the ionization energies and thus to guide the selection of the photon energies for the photoionization in the experiment.[43−45]

In detail, experiments conducted with $CH_3OH{-}O_2$ ices at 11.08 eV identify relevant ions at m/z = 47 but not m/z = 63 (Figures 4 and S4). Figure 4a shows a pronounced sublimation event at 190 K for the $CH(OH)_2^+$ fragment that is observed with photoionization at 11.08 and 11.00 eV; at the latter photon energy, the peak intensity is reduced sixfold. The large decrease in signal intensity between these photon energies from 2300 ± 400 counts to 370 ± 100, respectively, is a strong indication that the dissociative photoionization process is extremely close to its threshold during photoionization at 11.00 eV. The signal is not observed with 10.87 or 10.70 eV photons. While ions were detected at m/z = 63 (Figure S4), they are detectable at 10.70 eV and above and are therefore unlikely to be linked to **1**. The molecular formula of the m/z = 47 fragment was substantiated with the use of isotopically labeled methanol (Figure 4b). The peak was found to undergo an isotopic mass shift to m/z = 48 in $^{13}CH_3OH{-}O_2$ ice, confirming the presence of *exactly one* carbon atom in the fragment, and to m/z = 50 in CD_3OD-O_2 ice, confirming the inclusion of *exactly three* hydrogen atoms in the fragment. The isotopic labeling results with ^{13}C and D account for 15 amu that is comprised of carbon and three hydrogen atoms in the unlabeled species; hence, the difference of 32 amu must then be two oxygen atoms because this ice contains only carbon, hydrogen, and oxygen. The identified fragment molecular formula of CH_3O_2 agrees with the predicted dissociation for vertical ionization of **1** (Figure 2) and exhibits the predicted response to changes in the wavelength. Therefore, this signal is used here to identify **1** sublimating from the ice during TPD.

Having identified the presence of compound **1**, we focus now on the preparation of compounds **2** and **3**. The predicted ionization energies (9.77−9.95 eV for **2**, 9.65−9.87 eV for **3**) of these isomers suggest that no ions should be detectable at 9.50 eV, but both isomers should be detectable at energies greater than 9.95 eV. Figure 5 shows that with the photon energy in excess of adiabatic ionization, there are two peaks observable for m/z = 64. With 10.86, 10.82, 10.48, and 10.25

https://doi.org/10.1021/jacs.4c02637
J. Am. Chem. Soc. 2024, 146, 12174−12184

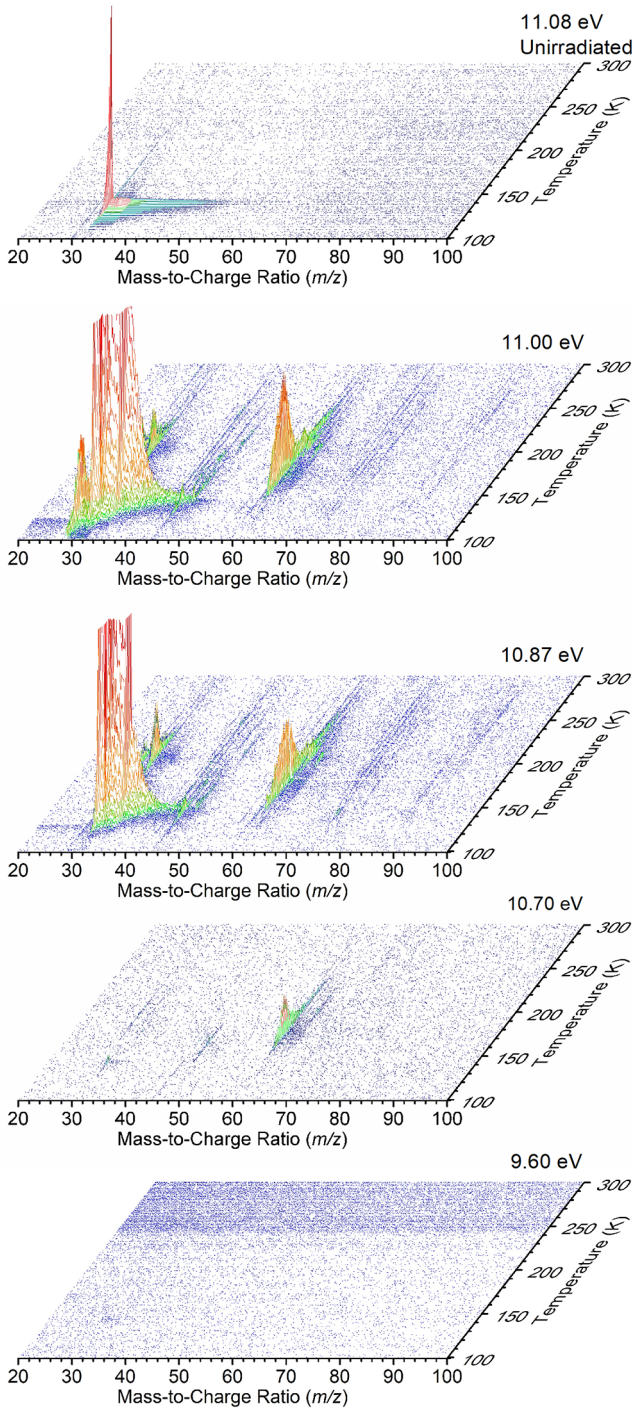

Figure 3. Mass spectra measured during the TPD of $CH_3OH{-}O_2$ ice. The mass spectra of ice are plotted as a function of temperature for measurements of unirradiated ice studied at 11.08 eV and irradiated ices with photons of 11.00, 10.87, 10.70, and 9.60 eV. The unirradiated ice is shown with a vertical axis scaled by 1/100 to show the entire methanol peak.

eV photoionization, a peak for m/z = 64 is found at 170 K and a second at 200 K, although it is weak with 10.25 eV photons. The two sublimation events found for m/z = 64 can be distinguished based on their distinct unimolecular decomposition barriers as gas-phase radical cations. Figure 6a shows that the profile of the peak at 200 K is found to be identical for m/z = 31 or 64, while the peak at 170 K is found only for m/z = 64. Verification of the molecular formulas is necessary for the clear identification of **2** and **3**.

Isotopic substitution is employed to determine the molecular formulas of the peaks at m/z = 64 and 31. The peak at 170 K is obstructed by coincident masses in ices containing CD_3OD (Figure 6b) and $^{13}CH_3OH$ (Figure 6c), but it is verified by a 4 amu increase in mass in $CH_3OH{-}^{18}O_2$ ice and an increase in mass by 6 amu when produced in the $CH_3{}^{18}OH{-}^{18}O_2$ ice. This demonstrates the presence of three atoms of oxygen in the molecules produced without isotopic substitution, which together account for 48 amu of mass in the 64 amu molecule. The remaining 16 amu can then only be attributed to the presence of one carbon and four hydrogen atoms. With the verification of the molecular formula represented by this peak and its lack of fragmentation, this peak can be assigned to **2**. Figure 6 shows that the more intense 200 K peak is highly visible in all isotopically labeled experiments, along with its fragment. In each experiment, these peaks appear at the appropriate mass for parent $CH_4O_3^{\bullet+}$ and fragment CH_3O^+, while the difference in mass between the parent and fragment is consistent with the elimination of $\dot{O}OH$. With knowledge of the molecular formulas of the peaks at m/z = 64 and the m/z = 31 fragment, the peak at 170 K can be assigned to **2**, while the sublimation event at 200 K is attributed to **3**.

3. DISCUSSION

The dissociative photoionization of **3** provides a unique opportunity to investigate its formation mechanism in unprecedented detail. In Scheme 2, reactions [1a], [1b],[46] and [2][47] are proposed as sources of radical intermediates.

$$CH_3OH \rightarrow \dot{C}H_2OH + \dot{H},\ [\Delta H_r^\circ\ (0\ K) = 395.8 \pm 0.7\ kJ\ mol^{-1}] \quad (1a)$$

$$CH_3OH \rightarrow CH_3\dot{O} + \dot{H},\ [\Delta H_r^\circ\ (0\ K) = 435.4 \pm 0.7\ kJ\ mol^{-1}] \quad (1b)$$

$$O_2 + \dot{H} \rightarrow \dot{O}OH,\ [\Delta H_r^\circ\ (0\ K) = -200.9 \pm 0.2\ kJ\ mol^{-1}] \quad (2)$$

These reactions all require energetic initiation, experimentally provided by energetic electrons simulating secondary particles produced by the GCRs. Since [1a] and [1b] are both endoergic, these reactions must be initiated while the ice is undergoing irradiation at 5 K. Once either [1a] or [1b] occurs due to the impact of an energetic electron, a hydrogen atom is ejected, reaction [2] can then occur through recombination of the released hydrogen atom with molecular oxygen.[48] Reactions [1a], [1b], and [2] produce three radicals that can undergo barrierless radical−radical recombination via reactions [3] and [4].

$$\dot{C}H_2OH + \dot{O}OH \rightarrow CH_2(OH)OOH \quad (3)$$

$$CH_3\dot{O} + \dot{O}OH \rightarrow CH_3OOOH \quad (4)$$

The sequence of reactions shown here is a well-documented mechanism in interstellar ice, which is the simplest mechanism that can complete the synthesis of **2** or **3**. During TPD, dissociative photoionization [5] of **3** then produces the hydroxymethyl cation (CH_2OH^+) and the hydroperoxyl radical ($\dot{O}OH$).

https://doi.org/10.1021/jacs.4c02637
J. Am. Chem. Soc. 2024, 146, 12174−12184

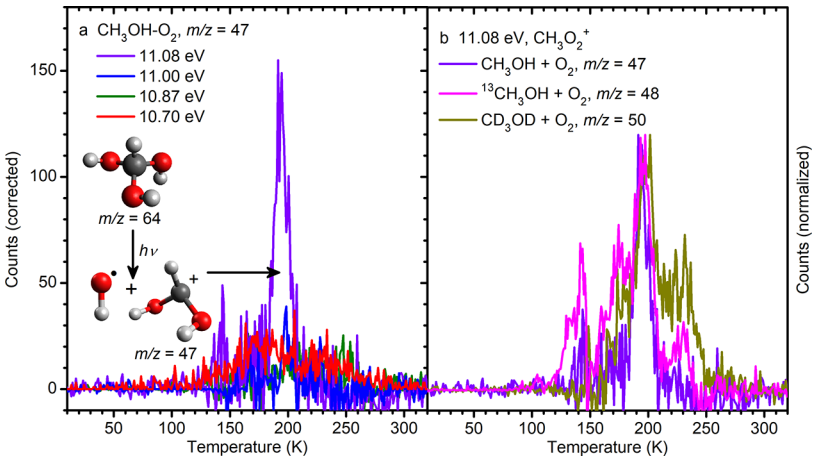

Figure 4. TPD profile for the fragment of $CH(OH)_3$. A peak is observed for m/z = 47 with photoionization above 11.00 eV but not below, confirming the 11.03 ± 0.04 eV appearance energy predicted for the dissociative photoionization of $CH(OH)_3$ to yield $CH(OH)_2^+$. Isotopic labeling reproduced the peak at 200 K assigned to the $CH(OH)_2^+$ fragment.

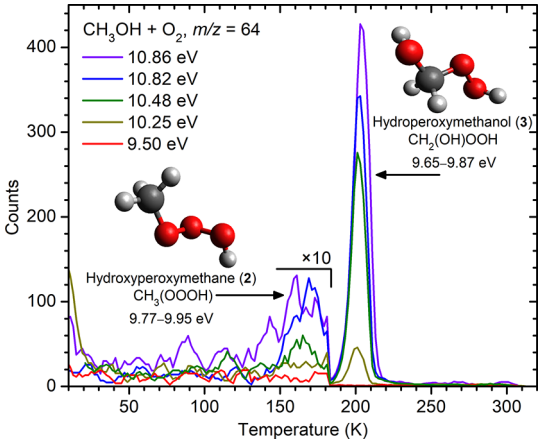

Figure 5. TPD profile for m/z = 64. Signal for m/z = 64 in $CH_3OH–O_2$ ices was observed with a range of photoionization energies. At 9.50 eV, neither of the two peaks is apparent.

$$CH_2(OH)OOH\ (\mathbf{3}) + h\nu \rightarrow CH_2OH^+ + \dot{O}OH + e^- \quad (5)$$

$$CH(OH)_3\ (\mathbf{1}) + h\nu \rightarrow CH_2OH^+ + \dot{O}OH + e^- \quad (6)$$

The CH_2OH^+ fragment contains only atoms originating from CH_3OH, and OH contains only oxygen from molecular oxygen deposited to form the ice. This partitioning of the reactants into known fragments is a powerful tool for determining the reaction mechanism. During TPD of $CH_3OH–{}^{18}O_2$ ices (Figure 6d), the peaks identified for **2** and **3** both appear only at m/z = 68 and must therefore be exclusively the $CH_4{}^{16}O^{18}O_2$ isotopomer, and the CH_2OH^+ fragment was only found at m/z = 31 as $CH_2{}^{16}OH^+$ without a signal at m/z = 33 for $CH_2{}^{18}OH^+$ (Figures S5 and S6). This shows that the structure must be $CH_2({}^{16}OH){}^{18}O_2H$, which is consistent with the proposed mechanism. Therefore, the hydroperoxyl moiety (−OOH) can be produced exclusively by the inclusion of intact O_2, and the hydroxyl moiety (−OH) can only come from methanol. Conversely, dissociation of $CH_2({}^{18}OH){}^{16}O{}^{18}OH$, which has the same mass as $CH_2({}^{16}OH){}^{18}O_2H$, differing only in the position of the two ^{18}O atoms, would dissociation to yield $^{16}\dot{O}{}^{18}OH$ and unobserved $CH_2{}^{18}OH^+$. This shows that no detectable

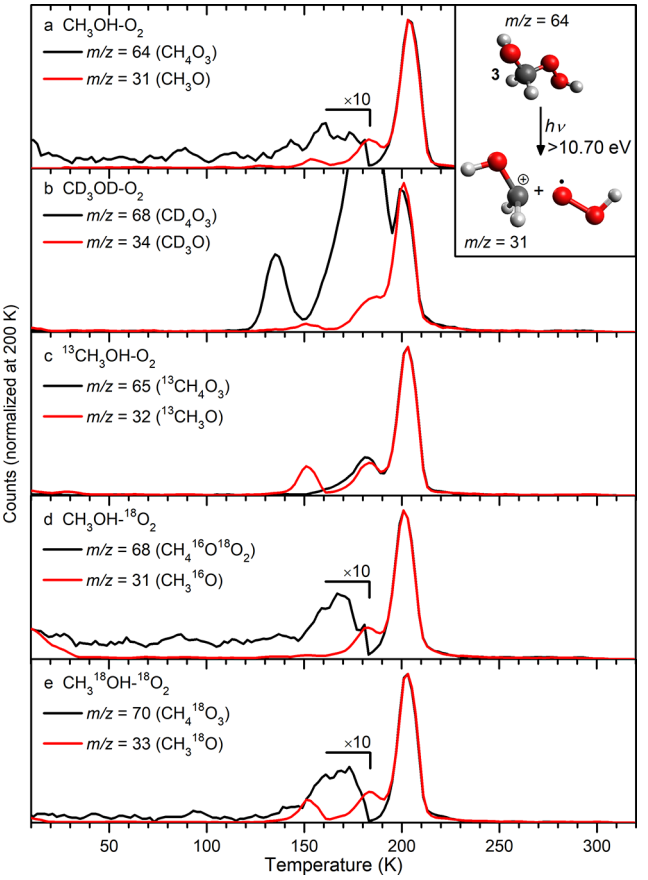

Figure 6. The 10.86 eV photoionization TPD profiles of isotopomers of $CH_4O_3^+$ and CH_3O^+. These TPD profiles are all shown after normalization of the peak at 200 K. This peak is observed for all studied isotopomers of $CH_4O_3^+$, confirming the assignment of this molecular formula. The peak at 170 K is observed without obstruction in both $CH_3OH–{}^{18}O_2$ and $CH_3{}^{18}OH–{}^{18}O_2$ ices. Furthermore, the consistent match of this peak with CH_3O^+ shows that this sublimation event is accompanied by fragmentation of the specific isomer of $CH_4O_3^+$ upon sublimation at 200 K.

reactions take place that result in the formation of an ^{18}O-containing hydroxyl in **3** in the present experiments. Due to the lack of fragmentation, the formation mechanism of **2** is less

https://doi.org/10.1021/jacs.4c02637
J. Am. Chem. Soc. 2024, 146, 12174−12184

certain. However, the fact that this isomer is found exclusively at m/z = 68 in the $CH_3{}^{16}OH{-}{}^{18}O_2$ ice is a strong indication that it also results from the radical−radical recombination mechanism involving reactions 1b, [2], and [4]. This would explain why two—and only two—^{18}O atoms can be incorporated into these isomers.

The quality of the agreement between experiment and theory demonstrated by these radical cation dissociation thresholds cannot be understated. The CCSD(T)/CBS//ωB97X-D/aug-cc-pVTZ calculated appearance energy of the CH_2OH^+ fragment from **3** is 10.70 ± 0.04 eV (Figures S7 and S8), which agrees with the experimentally observed onset of this fragment at 10.70−10.87 eV. The measured onset is also in agreement with prior CBS-QB3 calculations of the adiabatic ionization energy predicting the 10.7 eV value and accompanying observed onset at approximately 10.6 eV during the detection of internally hot neutral molecules, resulting in a reduction in the observable appearance energy in this earlier experiment.[7] Additionally, the predicted threshold for dissociation of **1** to yield $CH(OH)_2^+$ at 11.03 ± 0.04 eV practically coincides with the detected threshold at 11.00 eV. The close agreement is due to the high accuracy of the composite CCSD(T)/CBS//ωB97X-D/aug-cc-pVTZ method used in the calculations. Nevertheless, the computed low barrier separating $\mathbf{1b}^{\bullet+}$ from the dissociation products (Figure 2), only 6 ± 4 kJ mol^{-1}, brings some uncertainty as to whether the bound state exists. Experimental observations show that with photoionization at 11.00 eV, which is theoretically below the dissociation threshold (which includes corrections for Stark and thermal effects), resulted in a small signal for the $CH(OH)_2^+$ fragment, though no peak was identified for the parent at m/z = 64. While it cannot be ruled out that there is a bound cationic state at the temperature where **1** sublimes (190 K), there is no evidence that such a bound state exists.

A study of the minimum-energy conformers of a series of molecules $CH_{4-n}(OH)_n$ (n = 2, 3, 4) shown in Figure 1, i.e., methanediol ($CH_2(OH)_2$), **1**, and methanetetrol ($C(OH)_4$, Table S3), reveals the effects of the hydroxyl groups on each other. While these molecules demonstrate similar O−H and C−H bond lengths, the C−O bond length decreases as the number of hydroxyl groups increases and is ultimately 3 pm shorter in methanetetrol than in methanediol. This reproduces, at a higher level of theory, earlier results on these and similar multiply substituted methanes, indicating that the hydroxyl groups are mutually reinforcing in the neutral molecules, despite of the ready dissociation of the corresponding radical cations.[33] The greater steric repulsion between nonbonding lone pairs—valence shell electron pair repulsion (VSEPR)[49] theory—is a major factor affecting the bond angles across these species. The hydroxyl groups of methanediol experience mutual repulsion and are separated by an OCO angle of 112.6°, while the reduced repulsion produced by hydrogen results in reduced OCH and HCH bond angles of 105.3 and 110.2°, respectively. The conformer of **1** found to be most stable has hydroxyl groups in a *trans*−*gauche*−*gauche* (*tgg*) conformation (**1a**), while the *tgg*′ (**1b**, +5 kJ mol^{-1}) and *ggg* (**1c**, +10 kJ mol^{-1}) conformers were also identified as local minima. The orientation of these groups is relevant because the *trans* conformation orients the nonbonding pairs toward other methane substituents, unlike the *gauche* conformation. The *tgg* conformer of **1** shows that orienting the *gauche* hydrogen to face the *trans* oxygen increases repulsion and increases the OCO bond angle from 113.0 to 109.4°. Again, according to VSEPR theory, the adjacent hydroxyl groups of methanetetrol with nonbonding electrons oriented toward each other are expected to experience greater mutual repulsion and are found computationally to be separated by an OCO angle of 113.7°. Adjacent groups with the hydrogen directed toward nonbonding electrons exhibit reduced repulsion and a bond angle of 107.4°. These deviations from the ideal tetrahedral angle of 109.5° demonstrate a distorted tetrahedral structure that preserves some symmetry elements. Because this structure retains the symmetry of the C_2 (180°) rotation and S_4 (90°) rotation-reflection operations (Figure 1), this molecule is representative of the uncommon S_4 point group.

4. CONCLUSIONS

Methanetriol (**1**, $CH(OH)_3$) has, until now, proven to be an elusive molecule, and its identification opens the possibility for investigating its chemistry and spectroscopy. The irradiation dose of the $CH_3OH{-}O_2$ ice that resulted in **1** exceeds what is expected of the typical molecular cloud with a lifetime of up to 5 × 10^7 years. However, longer-lived cometary ice can be subjected to GCR exposure, totaling an irradiation dose sufficient to produce methanetriol. Comets are typically composed of 2−7% methanol, which has been detected in abundance in the coma of comet 67P/Churyumov-Gerasimenko.[50,51] Because they contain both reactants in an environment subjected to constant irradiation, comets are ideal candidates for the detection of **1** in space. The formation of **2** and **3** here results from reactions of the hydroperoxyl radical (ȮH) formed by hydrogen transfer from methanol. The infrared inactivity of molecular oxygen (O_2) makes it difficult to detect in interstellar ice, but it has been directly measured in the coma of comet 67P to have an abundance of 3.8 ± 0.9% relative to water (H_2O).[52] Methanol is easy to detect through astronomy in the infrared, and it has been found to be present in both cometary and interstellar ices with a typical abundance of 3−12% relative to H_2O.[53] The irradiation dose employed in the present preparation of **2** and **3** is comparable to that experienced by a typical interstellar molecular cloud over the course of 10^6−10^7 years, well within the lifetime of typical molecular clouds.[54] It is highly likely that both isomers **2** and **3** are present in the interstellar medium, given the abundance of the reactants and the initiating energy sources.

While warm compared to the ISM, the stratosphere of Earth and the upper atmospheres of some planets and moons contain icy clouds exposed to both GCRs and solar ultraviolet (UV) radiation. Methanol is the second most abundant organic molecule in the atmosphere, being produced via **2** as an intermediate.[55] Stratospheric ices, particularly in the polar regions, are cold enough to condense methanol, and where both solar UV and GCR radiation can initiate reactions with atmospheric O_2 or with ambient OH also produced by energetic initiation. The potential for terrestrial stratospheric ices to act as hosts for these reactions bears significant attention, as all three isomers of CH_4O_3 discussed here represent functional groups known or suspected to participate in secondary organic aerosol production. Furthermore, the unknown potential for the production of **1** through solar UV radiation is a topic with the potential to impact planetary science on Earth along with any planet with an oxygen-rich atmosphere.

https://doi.org/10.1021/jacs.4c02637
J. Am. Chem. Soc. 2024, 146, 12174−12184

5. METHODS AND MATERIALS

5.1. Experimental Section. Experiments utilizing synchrotron radiation (11.08, 11.00, 10.87, and 10.70 eV) were conducted at the Shanghai-Hawaii-Hefei Advanced Research Center (SHHARC), located at the National Synchrotron Radiation Laboratory (NSRL) in Hefei, China, on the BL03U beamline for astrochemistry.[56] This instrument consists of a hydrocarbon-free stainless steel ultrahigh vacuum (UHV) chamber with pressures maintained in the ultrahigh vacuum regime. A closed cycle helium refrigerator (Sumitomo Heavy Industries, RDK-415E) is used to maintain a mirror-polished silver wafer (12.6 × 15.1 mm) at 4.8 ± 0.1 K. Ices were prepared by delivering gases through 10 mm diameter glass capillary arrays directed at the wafer at a partial pressure of 10^{-8} Torr for each gas. Deposition used the same pressure of each component gas to approach a 1:1 ratio of $[CH_3OH]/[O_2]$. Samples used at the SHHARC include methanol (CH_3OH, TEDIA, 99.98%; $^{13}CH_3OH$, Aladdin Scientific Corp., 99.0 atom % ^{13}C; CD_3OD, Aladdin Scientific Corp., 99.8 atom % D) and molecular oxygen (O_2, Air Liquide, 99.999%). Prior to any experiments using CD_3OD, all tubing and capillary arrays used to deliver the vapor to the wafer were purged with CD_3OD to allow any isotope exchange and loss of deuterium to occur prior to experimental ice deposition. The thickness of the deposited ice was measured based on the reflected intensity of a helium−neon laser (CVI Melles-Griot, 25-LHP-230, 632.8 nm) at a 2° angle of incidence. Variations in the reflected laser resulting from the interference during deposition indicate an average ice thickness of 750 ± 50 nm. In calculating this thickness, the ice index of refraction was approximated by the average of the indexes of refraction of the two components, 1.33 ± 0.04 for CH_3OH and 1.25 for O_2 in amorphous ices.[57,58]

For the purpose of simulating electron irradiation computationally, densities of 1.01 ± 0.03 g cm^{-3} at for CH_3OH and 1.5 ± 0.1 g cm^{-3} for O_2 were used as an approximation for the unknown density of the mixed ices.[58,59] Average electron penetration depth was predicted to be 230 ± 20 nm in CH_3OH-O_2 ice, 228 ± 20 nm in $^{13}CH_3OH-O_2$ ice, and 224 ± 20 nm in CD_3OD-O_2 with the aid of Monte Carlo simulations conducted in CASINO 2.42.[60] The average penetration depth is significantly less than the ice thickness (750 ± 50 nm) to prevent interactions between the ice and the silver substrate from being initiated by energetic electrons. These experiments studied ices that were exposed to 1000 nA of electron current for 60 min, resulting in energetic irradiation doses totaling 152 ± 24 eV per molecule.

The synchrotron vacuum ultraviolet photoionization reflectron time-of-flight mass spectrometer (SVUV-PI-ReToF-MS) utilized in this research has been discussed in detail previously.[56] Temperature-programmed desorption (TPD) at a rate of 1 K min^{-1} was employed. During TPD, the VUV light was passed 1−2 mm above the surface of the ice to photoionize subliming molecules. Ions are mass-analyzed in a reflectron time-of-flight mass spectrometer and detected on a microchannel plate (MCP) detector (Jordan TOF Products). The MCP signal was amplified (Ortec, 9306) prior to discrimination and amplification to 4 V (Advanced Research Instruments Corp., F-100TD) and recorded by a multichannel scaler (FAST ComTec, P7889). Ion arrival times were recorded to 3.2 ns accuracy. Mass spectra were repeated at a rate of 15 kHz until the temperature of the sample reached 320 K. The SVUV light is quasi-continuous, requiring pulsed extraction of ions into the mass spectrometer. This was accomplished by electronic pulsing of the extraction grid between a small repelling voltage (+2 V) and an extraction voltage (−68 V), where extraction marks the beginning of each cycle of the ReToF-MS (S9−S12).

Experiments utilizing four-wave mixing to generate vacuum ultraviolet (VUV) light (10.86, 10.82, 10.48, 10.25, and 9.50 eV) were carried out at both the W. M. Keck Research Laboratory in Astrochemistry of the University of Hawaii at Manoa.[61−63] Experimental procedures and data from these experiments have been discussed previously and differ only slightly from the experimental procedure detailed above.[11] The implementation of the two instruments for these experiments is identical except for the use of four-wave mixing VUV generation, and Fourier transform infrared spectrometry in Hawaii, while synchrotron radiation without the use of FTIR is employed at Hefei. This is vital because four-wave mixing, as implemented here, is easily tunable to a maximum photon energy of 10.86 eV and can access higher energy photons only at 11.10 eV; however, synchrotrons do not face the same challenges as dye lasers and are continuously tunable through the range inaccessible by four-wave mixing. Experimental parameters are also the same with two exceptions: ices were deposited to 500 ± 30 nm thickness, and irradiation was limited to 50 nA for 30 min, corresponding to a dose of 3.8 ± 0.6 eV per molecule.

5.2. Computational. All computations started with a geometry optimization and vibrational frequency analysis at the ωB97X-D/aug-cc-pVTZ level of theory for all neutral molecules in the Gaussian 09 computational package.[64] The wave functions were always checked for stability in the DFT calculations of geometries and vibrational frequencies to ensure that the results correspond to the ground electronic states. Optimized structures were used to carry out single-point CCSD(T) calculations with extrapolation to the complete basis set limit, CCSD(T)/CBS, using the MOLPRO 2015 package.[65] The CCSD(T) calculations were monitored for T1 diagnostics to verify the absence of a significant multireference character of the wave functions, and no problematic cases were observed. Local minima for cations were optimized by starting from the optimized structures of the corresponding neutral molecules. All neutral and cationic structures were confirmed to have all real vibrational frequencies, and all optimized transition states were confirmed to have only one imaginary frequency corresponding to the reaction coordinate. The investigated structures included all plausible configurations for the CH_4O_3 system (Figure S13).

■ ASSOCIATED CONTENT

Supporting Information

The Supporting Information is available free of charge at https://pubs.acs.org/doi/10.1021/jacs.4c02637.

Computational results, including optimized Cartesian coordinates and energetics, supplementary TPD profiles, and experimental error analysis (PDF)

■ AUTHOR INFORMATION

Corresponding Authors

Tao Yang − *State Key Laboratory of Precision Spectroscopy, East China Normal University, Shanghai 200062, P. R. China; Collaborative Innovation Center of Extreme Optics, Shanxi University, Taiyuan, Shanxi 030006, P. R. China;* orcid.org/0000-0003-4101-2385; Email: tyang@lps.ecnu.edu.cn

Alexander M. Mebel − *Department of Chemistry and Biochemistry, Florida International University, Miami, Florida 33199, United States;* orcid.org/0000-0002-7233-3133; Email: mebela@fiu.edu

Ralf I. Kaiser − *Department of Chemistry, University of Hawaii at Manoa, Honolulu, Hawaii 96822, United States; W. M. Keck Research Laboratory in Astrochemistry, University of Hawaii at Manoa, Honolulu, Hawaii 96822, United States;* orcid.org/0000-0002-7233-7206; Email: ralfk@hawaii.edu

Authors

Joshua H. Marks − *Department of Chemistry, University of Hawaii at Manoa, Honolulu, Hawaii 96822, United States; W. M. Keck Research Laboratory in Astrochemistry, University of Hawaii at Manoa, Honolulu, Hawaii 96822, United States;* orcid.org/0000-0003-0492-2494

Xilin Bai − *State Key Laboratory of Precision Spectroscopy, East China Normal University, Shanghai 200062, P. R. China*
Anatoliy A. Nikolayev − *Samara National Research University, Samara 443086, Russia*
Qi'ang Gong − *State Key Laboratory of Precision Spectroscopy, East China Normal University, Shanghai 200062, P. R. China*
Cheng Zhu − *Department of Chemistry, University of Hawaii at Manoa, Honolulu, Hawaii 96822, United States; W. M. Keck Research Laboratory in Astrochemistry, University of Hawaii at Manoa, Honolulu, Hawaii 96822, United States*
N. Fabian Kleimeier − *Department of Chemistry, University of Hawaii at Manoa, Honolulu, Hawaii 96822, United States; W. M. Keck Research Laboratory in Astrochemistry, University of Hawaii at Manoa, Honolulu, Hawaii 96822, United States;* orcid.org/0000-0003-1767-897X
Andrew M. Turner − *Department of Chemistry, University of Hawaii at Manoa, Honolulu, Hawaii 96822, United States; W. M. Keck Research Laboratory in Astrochemistry, University of Hawaii at Manoa, Honolulu, Hawaii 96822, United States*
Santosh K. Singh − *Department of Chemistry, University of Hawaii at Manoa, Honolulu, Hawaii 96822, United States; W. M. Keck Research Laboratory in Astrochemistry, University of Hawaii at Manoa, Honolulu, Hawaii 96822, United States*
Jia Wang − *Department of Chemistry, University of Hawaii at Manoa, Honolulu, Hawaii 96822, United States; W. M. Keck Research Laboratory in Astrochemistry, University of Hawaii at Manoa, Honolulu, Hawaii 96822, United States*
Jiuzhong Yang − *National Synchrotron Radiation Laboratory, University of Science and Technology of China, Hefei, Anhui 230029, P. R. China;* orcid.org/0000-0002-7076-3412
Yang Pan − *National Synchrotron Radiation Laboratory, University of Science and Technology of China, Hefei, Anhui 230029, P. R. China;* orcid.org/0000-0002-9360-3809

Complete contact information is available at: https://pubs.acs.org/10.1021/jacs.4c02637

Notes

The authors declare no competing financial interest.

■ ACKNOWLEDGMENTS

This work was conducted under a Memorandum of Understanding (MOU) between the East China Normal University (ECNU), the University of Hawaii at Manoa (UHM), and the National Synchrotron Radiation Laboratory (NSRL) at the University of Science and Technology of China (USTC). The W. M. Keck Foundation and the University of Hawaii at Manoa financed the W. M. Keck Research Laboratory in Astrochemistry. T.Y. acknowledges the support from the National Natural Science Foundation of China (12034008, 12250003, 12274140, and 11874151), the Shanghai Natural Science Foundation (22ZR1421400), and the Program for Professor of Special Appointment (Eastern Scholar) at Shanghai Institutions of Higher Learning. The experiments of the Hawaii team were supported by the US National Science Foundation (NSF) Division for Astronomy (NSF-AST 2103269).

■ REFERENCES

(1) Hewitt, C. N.; Kok, G. L. Formation and Occurrence of Organic Hydroperoxides in the Troposphere: Laboratory and Field Observations. *J. Atmos. Chem.* **1991**, *12*, 181−194.
(2) Hua, W.; Chen, Z. M.; Jie, C. Y.; Kondo, Y.; Hofzumahaus, A.; Takegawa, N.; Chang, C. C.; Lu, K. D.; Miyazaki, Y.; Kita, K.; et al. Atmospheric Hydrogen Peroxide and Organic Hydroperoxides During PRIDE-PRD'06, China: Their Concentration, Formation Mechanism and Contribution to Secondary Aerosols. *Atmos. Chem. Phys.* **2008**, *8*, 6755−6773.
(3) Bian, H.; Zhang, S.; Zhang, H. Theoretical Study on the Atmospheric Reaction of CH_3O_2 with OH. *Int. J. Quantum Chem.* **2015**, *115*, 1181−1186.
(4) Lewis, T. R.; Blitz, M. A.; Heard, D. E.; Seakins, P. W. Direct Evidence for a Substantive Reaction Between the Criegee Intermediate, CH_2OO, and the Water Vapour Dimer. *Phys. Chem. Chem. Phys.* **2015**, *17*, 4859−4863.
(5) Muller, J. F.; Liu, Z.; Nguyen, V. S.; Stavrakou, T.; Harvey, J. N.; Peeters, J. The Reaction of Methyl Peroxy and Hydroxyl Radicals as a Major Source of Atmospheric Methanol. *Nat. Commun.* **2016**, *7*, 13213.
(6) Nguyen, T. B.; Tyndall, G. S.; Crounse, J. D.; Teng, A. P.; Bates, K. H.; Schwantes, R. H.; Coggon, M. M.; Zhang, L.; Feiner, P.; Millller, D. O.; et al. Atmospheric Fates of Criegee Intermediates in the Ozonolysis of Isoprene. *Phys. Chem. Chem. Phys.* **2016**, *18*, 10241−10254.
(7) Sheps, L.; Rotavera, B.; Eskola, A. J.; Osborn, D. L.; Taatjes, C. A.; Au, K.; Shallcross, D. E.; Khan, M. A. H.; Percival, C. J. The Reaction of Criegee Intermediate CH_2OO With Water Dimer: Primary Products and Atmospheric Impact. *Phys. Chem. Chem. Phys.* **2017**, *19*, 21970−21979.
(8) Anglada, J. M.; Sole, A. Tropospheric Oxidation of Methyl Hydrotrioxide (CH_3OOOH) by Hydroxyl Radical. *Phys. Chem. Chem. Phys.* **2018**, *20*, 27406−27417.
(9) Yan, C.; Krasnoperov, L. N. Pressure-Dependent Kinetics of the Reaction between CH_3O_2 and OH: TRIOX Formation. *J. Phys. Chem. A* **2019**, *123*, 8349−8357.
(10) Berndt, T.; Chen, J.; Kjaergaard, E. R.; Møller, K. H.; Tilgner, A.; Hoffmann, E. H.; Herrmann, H.; Crounse, J. D.; Wennberg, P. O.; Kjaergaard, H. G. Hydrotrioxide (ROOOH) Formation in the Atmosphere. *Science* **2022**, *376*, 979−982.
(11) Zhu, C.; Kleimeier, N. F.; Turner, A. M.; Singh, S. K.; Fortenberry, R. C.; Kaiser, R. I. Synthesis of Methanediol [$CH_2(OH)_2$]: The Simplest Geminal Diol. *Proc. Natl. Acad. Sci. U.S.A.* **2022**, *119*, No. e2111938119.
(12) Stary, F. E.; Emge, D. E.; Murray, R. W. Ozonization of Organic Substrates. Hydrotrioxide Formation and Decomposition to Give Singlet Oxygen. *J. Am. Chem. Soc.* **1976**, *98*, 1880−1884.
(13) Zhang, F.; Huang, C. Pressure-Dependent Kinetics of the Reaction between CH_3OO and OH Focusing on the Product Yield of Methyltrioxide (CH_3OOOH). *J. Phys. Chem. Lett.* **2019**, *10*, 3598−3603.
(14) Jungkamp, T. P. W.; Seinfeld, J. H. The Enthalpy of Formation of Trioxy Radicals ROOO (R = H, CH_3, C_2H_5). An Ab Initio Study. *Chem. Phys. Lett.* **1996**, *257*, 15−22.
(15) Lay, T. H.; Bozzelli, J. W. Enthalpies of Formation and Group Additivity of Alkyl Peroxides and Trioxides. *J. Phys. Chem. A* **1997**, *101*, 9505−9510.
(16) Koller, J.; Hodoscek, M.; Plesnicar, B. Chemistry of Hydrotrioxides. A Comparative Ab Initio Study of the Equilibrium Structures of Monomeric and Dimeric Hydrotrioxides (CH_3OOOH, $H_3SiOOOH$) and Hydroperoxides (CH_3OOH, H_3SiOOH). Relative Bond Strengths in and the as Phase Acidities of Hydrotrioxides and Hydroperoxides. *J. Am. Chem. Soc.* **1990**, *112*, 2124−2129.
(17) Francisco, J. S.; Williams, I. H. The Thermochemistry of Polyoxides and Polyoxy Radicals. *Int. J. Chem. Kinet.* **1988**, *20*, 455−466.

(18) Liang, Y. N.; Li, J.; Wang, Q. D.; Wang, F.; Li, X. Y. Computational Study of the Reaction Mechanism of the Methylperoxy Self-Reaction. *J. Phys. Chem. A* **2011**, *115*, 13534−13541.
(19) Stone, D.; Whalley, L. K.; Heard, D. E. Tropospheric OH and HO_2 Radicals: Field Measurements and Model Comparisons. *Chem. Soc. Rev.* **2012**, *41*, 6348−6404.
(20) Ryzhkov, A. B.; Ariya, P. A. A Theoretical Study of the Reactions of Parent and Substituted Criegee Intermediates With Water and the Water Dimer. *Phys. Chem. Chem. Phys.* **2004**, *6*, 5042.
(21) Zhu, C.; Kumar, M.; Zhong, J.; Li, L.; Francisco, J. S.; Zeng, X. C. New Mechanistic Pathways for Criegee-Water Chemistry at the Air/Water Interface. *J. Am. Chem. Soc.* **2016**, *138*, 11164−11169.
(22) Cui, X.; Li, H.; Wang, Y.; Hu, Y.; Hua, L.; Li, H.; Han, X.; Liu, Q.; Yang, F.; He, L.; et al. Room-Temperature Methane Conversion by Graphene-Confined Single Iron Atoms. *Chem.* **2018**, *4*, 1902−1910.
(23) Anglada, J. M.; Sole, A. Impact of the Water Dimer on the Atmospheric Reactivity of Carbonyl Oxides. *Phys. Chem. Chem. Phys.* **2016**, *18*, 17698−17712.
(24) IPCC *Climate Change 2021: The Physical Science Basis*; Cambridge Univ. Press, 2021.
(25) Lehn, J.-M.; Wipff, G.; Bürgi, H. Stereoelectronic Properties of Tetrahedral Species Derived from Carbonyl Groups. Ab Initio Study of the Hydroxymethanes. *Helv. Chim. Acta* **1974**, *57*, 493−496.
(26) Benson, S. W. Electrostatics, the Chemical Bond and Molecular Stability. *Angew. Chem., Int. Ed.* **1978**, *17*, 812−819.
(27) Baird, N. C. Nonadditive Effects of Polysubstitution in CH_4 and CH_3: A Test of ab Initio and Semiempirical MO Methods. *Can. J. Chem.* **1983**, *61*, 1567−1572.
(28) Leška, J.; Németh, E.; Loos, D. A Quantum-Chemical Study of Dehydration of Ortho Forms of Formaldehyde and Formic Acid. *ChemPlusChem* **1986**, *51*, 1819−1833.
(29) Böhm, S.; Senf, I.; Schädler, H. D.; Kuthan, J. A Theoretical Study of the Methanetriol Decomposition Mechanism. *Comput. Theor. Chem.* **1992**, *253*, 73−82.
(30) Grein, F.; Deslongchamps, P. The Anomeric and Reverse Anomeric Effect. A Simple Energy Decomposition Model for Acetals and Protonated Acetals. *Can. J. Chem.* **1992**, *70*, 1562−1572.
(31) Lathan, W. A.; Radom, L.; Hehre, W. J.; Pople, J. A. Molecular Orbital Theory of the Electronic Structure of Organic Compounds. XVIII. Conformations and Stabilities of Trisubstituted Methanes. *J. Am. Chem. Soc.* **1973**, *95*, 699−703.
(32) Böhm, S.; Antipova, D.; Kuthan, J. Study of Methanetriol Decomposition Mechanisms. *Int. J. Quantum Chem.* **1996**, *60*, 649−655.
(33) Menon, A. S.; Henry, D. J.; Bally, T.; Radom, L. Effect of Substituents on the Stabilities of Multiply-Substituted Carbon-Centered Radicals. *Org. Biomol. Chem.* **2011**, *9*, 3636−3657.
(34) Barić, D.; Maksić, Z. B. Additivity of the Correlation Energy in Some 3D Organic Molecules. *J. Phys. Chem. A* **2002**, *106*, 1612−1618.
(35) Toumi, I.; Yazidi, O.; Jaidane, N. E.; Al Mogren, M. M.; Francisco, J. S.; Hochlaf, M. Stereoisomers of Hydroxymethanes: Probing Structural and Spectroscopic Features upon Substitution. *J. Chem. Phys.* **2016**, *145*, 244305.
(36) Jasper, A. W.; Harding, L. B.; Knight, C.; Georgievskii, Y. Anharmonic Rovibrational Partition Functions at High Temperatures: Tests of Reduced-Dimensional Models for Systems with up to Three Fluxional Modes. *J. Phys. Chem. A* **2019**, *123*, 6210−6228.
(37) Bennett, C. J.; Hama, T.; Kim, Y. S.; Kawasaki, M.; Kaiser, R. I. Laboratory Studies on the Formation of Formic Acid (HCOOH) in Interstellar and Cometary Ices. *Astrophys. J.* **2011**, *727*, 27.
(38) Devane, W. A.; Hanus, L.; Breuer, A.; Pertwee, R. G.; Stevenson, L. A.; Griffin, G.; Gibson, D.; Mandelbaum, A.; Etinger, A.; Mechoulam, R. Isolation and structure of a brain constituent that binds to the cannabinoid receptor. *Science* **1992**, *258*, 1946−1949.
(39) Franco, B.; Blumenstock, T.; Cho, C.; Clarisse, L.; Clerbaux, C.; Coheur, P. F.; De Maziere, M.; De Smedt, I.; Dorn, H. P.; Emmerichs, T.; et al. Ubiquitous Atmospheric Production of Organic Acids Mediated by Cloud Droplets. *Nature* **2021**, *593*, 233−237.
(40) Permar, W.; Wielgasz, C.; Jin, L.; Chen, X.; Coggon, M. M.; Garofalo, L. A.; Gkatzelis, G. I.; Ketcherside, D.; Millet, D. B.; Palm, B. B.; et al. Assessing Formic and Acetic Acid Emissions and Chemistry in Western U.S. Wildfire Smoke: Implications for Atmospheric Modeling. *Environ. Sci.: Atmos.* **2023**, *3*, 1620−1641.
(41) McLafferty, F. W.; Tureek, F. *Interpretation of Mass Spectra*; University Science Books, 1993.
(42) Wang, J.; Nikolayev, A. A.; Marks, J. H.; McAnally, M.; Azyazov, V. N.; Eckhardt, A. K.; Mebel, A. M.; Kaiser, R. I. Quantum Tunneling Mediated Low-Temperature Synthesis of Interstellar Hemiacetals. *J. Phys. Chem. Lett.* **2023**, *14*, 6078−6085.
(43) Kendall, R. A.; Dunning, T. H.; Harrison, R. J. Electron Affinities of the First-Row Atoms Revisited. Systematic Basis Sets and Wave Functions. *J. Chem. Phys.* **1992**, *96*, 6796−6806.
(44) Stanton, J. F. Why CCSD(T) Works: A Different Perspective. *Chem. Phys. Lett.* **1997**, *281*, 130−134.
(45) Chai, J. D.; Head-Gordon, M. Long-Range Corrected Hybrid Density Functionals With Damped Atom-Atom Dispersion Corrections. *Phys. Chem. Chem. Phys.* **2008**, *10*, 6615−6620.
(46) Nguyen, T. L.; Stanton, J. F. A Steady-State Approximation to the Two-Dimensional Master Equation for Chemical Kinetics Calculations. *J. Phys. Chem. A* **2015**, *119*, 7627−7636.
(47) Ruscic, B.; Bross, D. Active Thermochemical Tables (ATcT) values based on ver. 1.130 of the Thermochemical Network; Argonne National Laboratory: Lemont, IL, 2023.
(48) Lü, Y.; Zhang, C.; Guo, Q.; Li, Y. An Accurate Many-Body Expansion Potential Energy Surface for HO_2 (X^2A'') by Extrapolation to the Complete Basis Set Limit and Quantum Dynamics of the Related Reaction $O(^3P)$ + $OH(^2\Pi)$. *J. Phys. B* **2023**, *56*, 135001.
(49) Bader, R. F. W.; Gillespie, R. J.; MacDougall, P. J. A Physical Basis for the VSEPR Model of Molecular Geometry. *J. Am. Chem. Soc.* **1988**, *110*, 7329−7336.
(50) Mumma, M. J.; Charnley, S. B. The Chemical Composition of Comets—Emerging Taxonomies and Natal Heritage. *Annu. Rev. Astron. Astrophys.* **2011**, *49*, 471−524.
(51) Le Roy, L.; Altwegg, K.; Balsiger, H.; Berthelier, J.-J.; Bieler, A.; Briois, C.; Calmonte, U.; Combi, M. R.; De Keyser, J.; Dhooghe, F.; et al. Inventory of the Volatiles on Comet 67P/Churyumov-Gerasimenko from Rosetta/ROSINA. *Astron. Astrophys.* **2015**, *583*, A1.
(52) Bieler, A.; Altwegg, K.; Balsiger, H.; Bar-Nun, A.; Berthelier, J. J.; Bochsler, P.; Briois, C.; Calmonte, U.; Combi, M.; De Keyser, J.; et al. Abundant Molecular Oxygen in the Coma of Comet 67P/Churyumov-Gerasimenko. *Nature* **2015**, *526*, 678−681.
(53) Boogert, A. A.; Gerakines, P. A.; Whittet, D. C. B. Observations of the Icy Universe. *Annu. Rev. Astron. Astrophys.* **2015**, *53*, 541−581.
(54) Yeghikyan, A. G. Irradiation of Dust in Molecular Clouds. II. Doses Produced by Cosmic Rays. *Astrophys.* **2011**, *54*, 87−99.
(55) Bates, K. H.; Jacob, D. J.; Wang, S.; Hornbrook, R. S.; Apel, E. C.; Kim, M. J.; Millet, D. B.; Wells, K. C.; Chen, X.; Brewer, J. F.; et al. The Global Budget of Atmospheric Methanol: New Constraints on Secondary, Oceanic, and Terrestrial Sources. *J. Geophys. Res. Atmos.* **2021**, *126*, No. e2020JD033439.
(56) Zhu, C.; Wang, H.; Medvedkov, I.; Marks, J.; Xu, M.; Yang, J.; Yang, T.; Pan, Y.; Kaiser, R. I. Exploitation of Synchrotron Radiation Photoionization Mass Spectrometry in the Analysis of Complex Organics in Interstellar Model Ices. *J. Phys. Chem. Lett.* **2022**, *13*, 6875−6882.
(57) Elsila, J.; Allamandola, L. J.; Sandford, S. A. The 2140 cm^{-1} (4.673 microns) Solid CO Band: The Case for Interstellar O_2 and N_2 and the Photochemistry of Nonpolar Interstellar Ice Analogs. *Astrophys. J.* **1997**, *479*, 818−838.
(58) Bouilloud, M.; Fray, N.; Bénilan, Y.; Cottin, H.; Gazeau, M. C.; Jolly, A. Bibliographic Review and New Measurements of the Infrared Band Strengths of Pure Molecules at 25 K: H_2O, CO_2, CO, CH_4, NH_3, CH_3OH, HCOOH and H_2CO. *Mon. Not. R. Astron. Soc.* **2015**, *451*, 2145−2160.
(59) Roder, H. M. The Molar Volume (Density) of Solid Oxygen in Equilibrium with Vapor. *J. Phys. Chem. Ref. Data* **1978**, *7*, 949−958.

https://doi.org/10.1021/jacs.4c02637
J. Am. Chem. Soc. 2024, 146, 12174−12184

(60) Drouin, D.; Couture, A. R.; Joly, D.; Tastet, X.; Aimez, V.; Gauvin, R. CASINO V2.42—A Fast and Easy-to-use Modeling Tool for Scanning Electron Microscopy and Microanalysis Users. *Scanning* **2007**, *29*, 92−101.
(61) Jones, B. M.; Kaiser, R. I. Application of Reflectron Time-of-Flight Mass Spectroscopy in the Analysis of Astrophysically Relevant Ices Exposed to Ionization Radiation: Methane (CH_4) and D_4-Methane (CD_4) as a Case Study. *J. Phys. Chem. Lett.* **2013**, *4*, 1965−1971.
(62) Abplanalp, M. J.; Förstel, M.; Kaiser, R. I. Exploiting Single Photon Vacuum Ultraviolet Photoionization to Unravel the Synthesis of Complex Organic Molecules in Interstellar Ices. *Chem. Phys. Lett.* **2016**, *644*, 79−98.
(63) Abplanalp, M. J.; Gozem, S.; Krylov, A. I.; Shingledecker, C. N.; Herbst, E.; Kaiser, R. I. A Study of Interstellar Aldehydes and Enols as Tracers of a Cosmic Ray-Driven Nonequilibrium Synthesis of Complex Organic Molecules. *Proc. Natl. Acad. Sci. U.S.A.* **2016**, *113*, 7727−7732.
(64) *Gaussian 09*, Revision D.01; Gaussian, Inc.: Wallingford CT, 2009.
(65) MOLPRO. *A Package of Ab Initio Programs*. Version 2015.1; University of Cardiff: Cardiff, UK, 2015.

https://doi.org/10.1021/jacs.4c02637
J. Am. Chem. Soc. 2024, 146, 12174−12184